ACS Sustainable Chemistry & Engineering

pubs.acs.org/journal/ascecg

Research Article

Molecular Materials through Microdroplets: Synthesis of Protein-Protected Luminescent Clusters of Noble Metals

Sandeep Bose, Amit Chatterjee, Shantha Kumar Jenifer, Biswajit Mondal, Pillalamarri Srikrishnarka, Debasmita Ghosh, Angshuman Ray Chowdhuri, M. P. Kannan, Sailaja V. Elchuri, and Thalappil Pradeep*

Cite This: *ACS Sustainable Chem. Eng.* 2021, 9, 4554−4563

Read Online

ACCESS | Metrics & More | Article Recommendations | Supporting Information

ABSTRACT: Atomically precise noble metal nanoclusters protected with proteins have emerged as a new research frontier in nanoscience due to their unique optical and chemical properties as well as promising applications. In the present work, we have employed an ambient electrospray technique to synthesize protein-protected luminescent clusters of gold and silver within the time scale of a few microseconds, which typically takes hours. In the absence of an electric field, the spray results in nanoparticles and no cluster formation was noticed. Synthesis of these clusters in microdroplets leads to severalfold enhancement in the rate of cluster formation. Spectroscopic investigations such as optical absorption, transmission electron microscopy, and matrix-assisted laser desorption ionization mass spectrometry confirm the molecular nature of the particles formed. Luminescence of electrospray-synthesized clusters shows multifold enhancement as compared to the clusters synthesized in the solution phase. Luminescence of the clusters synthesized in microdroplets increases with the distance traveled by the spray. The formation of clusters via electrospray affects the secondary structure of the protein, and its conformation is different from that of the parent protein. The Au@BSA cluster is utilized for in vitro imaging of retinoblastoma NCC-RbC-51 cells demonstrating a biological application of the resultant material. The absence of solvents and additional reagents enhances the sustainability of the method.

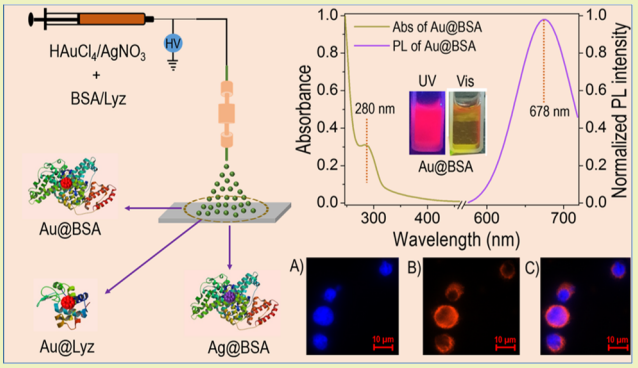

KEYWORDS: *nanoclusters, electrospray, microdroplets, conformation, retinoblastoma*

1. INTRODUCTION

Atomically precise luminescent clusters of noble metals are fascinating materials of immense promise.[1−8] Protein-protected clusters (PPCs) belong to a subclass of atomically precise noble metal clusters.[9−11] They possess many interesting properties, one of which is photoluminescence. Because of their unusual stability at ambient conditions, high quantum yield, and biocompatibility, these clusters are used in diverse areas,[12,13] such as sensing,[14−16] targeted drug delivery,[17,18] biolabeling,[19,20] multimodal imaging,[21−23] therapeutic applications,[24] and so forth. Bovine serum albumin (BSA), lysozyme (Lyz), human serum albumin, lactoferrin, and so forth are a few commonly used proteins to synthesize silver- and gold-based molecular clusters.[25−34]

Electrospray ionization (ESI) is a well-known technique for molecular ionization in mass spectrometry. In the recent past, the electrospray (ES) method has been used for chemical synthesis, which refers to the synthesis of molecules and materials in microdroplets formed in ES. This synthetic tool has been used previously for the generation of nanoparticles and nanostructures.[35−40] Synthesis of such materials in microdroplets leading to new properties such as luminescence in the visible region is yet to be explored. Luminescent materials, especially of biological importance such as PPCs prepared by this technique, will result in new and effective ways of processing such materials, for example, in the development of luminescent thin films. Reports of PPCs in solution suggest that reaction between noble metal ions and macromolecules is a multistep process.[32,41] These involve several complicated processes,[32] such as conformational changes in the protein, formation of metal ion−protein complex, reduction of metal ions, for example, Au^{3+} ions to Au^{0} via Au^{+}, the gradual evolution of clusters by sequential and slow addition of Au atoms to the core, and the formation of

Received: December 17, 2020
Revised: February 26, 2021
Published: March 16, 2021

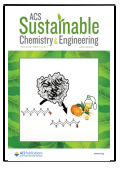

https://doi.org/10.1021/acssuschemeng.0c09145
ACS Sustainable Chem. Eng. 2021, 9, 4554−4563

Au−S bonds with cysteine as well as methionine residues of the protein, for protecting the metal core in the solution phase. All of these processes finally result in molecular clusters with intense luminescence. Such synthesis in the solution phase is a slow process and takes several hours to complete.

The fascinating thing about microdroplet reactions is that such processes occur in the timescale of microseconds[42,43] during which the droplets are produced and products are deposited on a collecting surface. Conformational changes of macromolecules and the formation of nanoparticles also occur in microdroplets under similar time scales.[35,39,44,45]

One of the interesting applications of these clusters is their use in bioimaging, especially for cancer cells. Retinoblastoma is a rare form of cancer that rapidly develops from the immature cells of the retina. It is the most common primary malignant intraocular cancer in children and almost exclusively found in young children. Retinoblastoma (Rb) arises due to mutation in the Rb gene leading to inactivated retinoblastoma protein.[46] It is a tumor suppressor protein, and its mutation leads to pediatric intraocular cancer. Rb could be caused either by germline mutation of the Rb1 gene or sporadic external factors and mutagens[47] and viruses like HP.[48] The Rb1 gene was the first tumor suppressor gene to be cloned.[49] Additionally, MYCN amplification could lead to Rb in 3% of tumors.[50,51] Rb tumors could originate from neuronal cells, glial cells, or stem cells of the retina. Besides, a Rb tumor is known to originate from the neuroectodermal cells.[52] The diagnosis of retinoblastoma is usually performed by fundoscopy. Imaging Rb tumors plays an important role in determining the therapeutic interventions as well as in detecting associated brain abnormalities, that is, intracranial tumor extension,[53,54] possible midline intracranial primitive neuroectodermal tumor,[55,56] and brain malformations in patients with 13q deletion syndrome.[57,58] Imaging Rb presents several challenges in front of clinicians due to its superficial position and the presence of fluids in the eye. Second, calcification of the vitreous bodies makes the tumor highly reflective, making imaging challenging.[59] Therefore, new molecules need to be synthesized, which can reach the posterior section of the eye and can image the Rb cells.

All of these together propose the possibility of making luminescent PPCs through microdroplets. In the present work, we have prepared ES-synthesized luminescent Au@BSA clusters, referred to as ES Au@BSA. Similar clusters, ES Au@Lyz and ES Ag@BSA, have also been prepared. We have utilized ES Au@BSA for in vitro imaging of Rb cells. The properties were compared with standard solution-processed samples, referred to as SP Au@BSA, SP Au@Lyz, and SP Ag@BSA. We have also observed that clusters formed by the spray show enhancement of luminescence when compared to those made through conventional SP methods.[28,29,31]

2. EXPERIMENTAL SECTION

2.1. Materials Required. Tetrachloroauric acid trihydrate ($HAuCl_4{\cdot}3H_2O$) was prepared in-house, starting from elemental gold. Silver nitrate ($AgNO_3$) and sodium hydroxide (NaOH) were purchased from Rankem, India. BSA was purchased from Sisco Research Laboratory. Lysozyme (Lyz) and Sodium borohydride ($NaBH_4$, 98%) were purchased from Sigma-Aldrich. Milli-Q water with 18.2 MΩ cm resistivity was used for all these experiments. Sinapic acid (99% purity) was used as the matrix for matrix-assisted laser desorption ionization mass spectrometry (MALDI MS) was purchased from Sigma-Aldrich. All chemicals for the experiment were used without further purification.

2.2. Solution Phase Synthesis of Au@BSA and Au@Lyz Cluster. Au@BSA was synthesized by mixing solutions of BSA and $HAuCl_4$ to get the final concentrations of 169 μM and 1.69 mM, respectively. At the optimized condition, the molar ratio of protein to Au^{3+} was 1:10. The total volume of the solution was 1 mL. To this, 100 μL of 1 M NaOH was added. The resulting mixture was stirred vigorously for 24 h until the solution became golden brown. Similarly, for Au@Lyz, similar concentration ratios of Au^{3+} and Lyz were used and the solution was stirred for 12 h. Both the solutions were freeze-dried and stored at 4 °C for later use. Microdroplets-based synthesis of PPCs will be presented in a later section.

2.3. Solution Phase Synthesis of Ag@BSA Cluster. For Ag@BSA synthesis, an aqueous solution of $AgNO_3$ and BSA having concentrations of 169 μM and 1.69 mM, respectively, were mixed. To this, 100 μL of 1 M NaOH was added. About 1 μL of 0.05 M $NaBH_4$ was added to the resulting mixture and stirred for 30 min until the solution turned golden brown. The sample was freeze-dried and stored at 4 °C for later use.

2.4. MALDI MS of the ES Au@BSA Cluster. MALDI MS of the ES Au@BSA cluster was carried out using a Voyager-DE PRO Biospectrometry Workstation from Applied Biosystems. A pulsed N_2 laser of 337 nm wavelength was used for ionizing the sample. Sinapic acid was chosen as the matrix. Matrix solution was prepared by using a mixture of acetonitrile and 0.1% trifluoroacetic acid in the ratio 1:3 in milli-Q water. About 5 μL of the analyte was mixed thoroughly with 50 μL of the matrix solution in a microcentrifuge tube. About 10 μL of the resulting mixture was spotted on the sample plate and air-dried before the measurement.

2.5. Quantum Yield Measurement of the Solution-Processed (SP) and ES Sample. For the red luminescent Au@BSA, Ag@BSA, and Au@Lyz, the PL quantum yield (QY) was calculated using Rhodamine 6G as a standard (QY = 95%, λ_{exc} = 488 nm). A freshly prepared solution was used to avoid errors. At this excitation wavelength, the absorbance values of both the dye and the clusters were adjusted to be the same. Photoluminescence (PL) spectra were recorded for the solutions with the same absorbance, and areas of the PL curves were calculated. Integrated PL intensities versus the corresponding absorbance values were plotted and fitted with a straight line to obtain two slopes which were utilized for determining the QY, using the established equation

$$\phi_{cluster} = \phi_{dye}(K_{cluster}/K_{dye}) \times (\text{R. I.})_{cluster}^{2}/(\text{R. I.})_{dye}^{2}$$

where $K_{cluster}$ and K_{dye} are the straight-line slopes and $(\text{R.I.})_{cluster}$, $(\text{R.I.})_{dye}$, and $\Phi_{cluster}$, Φ_{dye} are the refractive indices of the solvents and quantum yields of the clusters and the dye, respectively.

2.6. Effect of pH Change and Time-dependent Stability of Clusters. The pH of the cluster was adjusted by the addition of aq. NaOH or HCl dropwise. The change in the pH of the solution was measured by a digital pH meter. PL intensities of the samples were measured using a fluorimeter. Time-dependent luminescence intensity measurements were performed for 6 months at an interval of 30 days to check the stability of the clusters.

2.7. Cellular Uptake Studies by Fluorescence Microscopy. NCC-RbC-51 cell lines were procured from Riken cell bank, Japan. The cells were maintained in RPMI 1640 medium with 10% fetal bovine serum at 37 °C in a 5% CO_2 humidified incubator. These cells were incubated with ES Au@BSA clusters, and the uptake studies were performed for a period of 1 and 24 h. After incubation, the cell lines in the medium were centrifuged and the suspension cells were taken for analysis. The cells were mounted on a mounting medium containing Hoechst 33342 to stain the nuclei. These cells were covered with a coverslip and kept for further imaging. An optimized concentration of 1 mg/mL ES Au@BSA was used for uptake studies.

3. RESULTS AND DISCUSSION

3.1. Microdroplets-Based Synthesis. A schematic of the experimental setup is shown in Figure 1. In the present experiment, an aqueous solution of 169 μM $HAuCl_4$ was mixed with 1.69 mM proteins (BSA/Lyz) at 1:1 (v/v) ratio.

https://doi.org/10.1021/acssuschemeng.0c09145
ACS Sustainable Chem. Eng. 2021, 9, 4554−4563

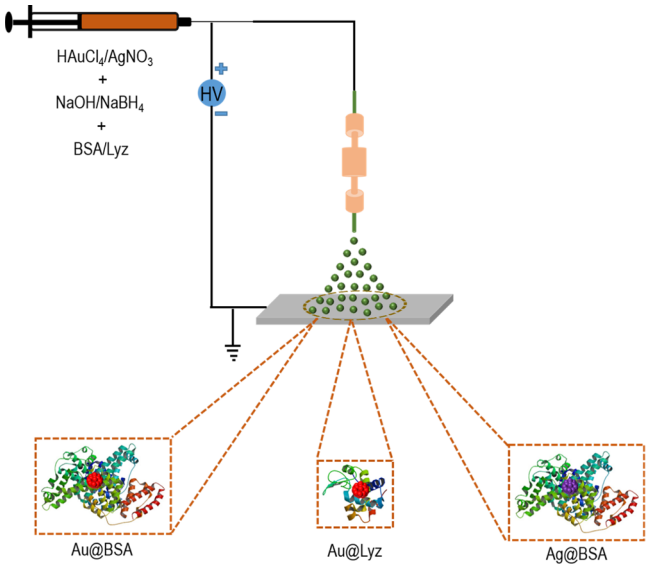

Figure 1. Schematic of the experimental setup utilized to synthesize the clusters by electrospray deposition.

About 100 μL of 1 M NaOH was added to the resulting mixture, and the solution was electrosprayed. A home-built nano-electrospray ionization source was used to direct the charged microdroplets of the resulting mixture. The spray was performed using a Hamilton syringe (1 mL) connected to a capillary delivering liquid at a constant flow rate of 5 μL/min. The potential applied to the tip of the needle was in the range of 4.5−5.0 kV. About 1% methanol was used for better ionization of the charged droplets. During electrospray, the reaction between the precursors takes place in the micro-droplets resulting in the formation of luminescent PPCs. This is because during electrospray, solvent evaporation occurs and the electrospray product get deposited on the substrate as a solid. Once it is converted to the solid phase from the aerosol, it is not likely to react with the ligands. Thus, the reaction can only occur during its travel from the tip to the substrate. The reaction product was collected on a conducting glass slide, washed with water, and used for further experiments. The spectroscopic characterizations were performed immediately after synthesis within a time span of 5−10 min. We have varied the applied electric field to observe the change in the luminescence properties of the cluster. Beyond the threshold potential (4.5−5 kV) necessary for electrospray under the present conditions, further increase did not lead to a change in luminescence (Figure S1). Two clusters, namely, ES Au@BSA and ES Au@Lyz, were prepared by this method.

We have selected the proteins BSA and Lyz for electrospray synthesis because these are widely used as model proteins for cluster synthesis. These clusters are biocompatible which enables them to be used in applications such as sensing, biolabeling, multimodal imaging, targeted drug delivery, and so forth unlike thiol-protected noble metal clusters which are toxic to cells, limiting their use in biological mediums for sensing, imaging, and therapeutic purposes. These are also stable in solution as well as in the solid state. These materials can also be used in different physiological conditions. This is why we have selected PPC over other thiol-protected noble metal clusters.

We have selected ES Au@BSA, ES Ag@BSA, and ES Au@Lyz for comparison in our experiments because all of these materials are equally useful for applications in biological mediums. We also want to show that the method is not selective to a particular protein or a particular metal and can be applied universally for the synthesis of different PPCs. Moreover, we want to show that different molecular weights of the proteins (BSA and Lyz) do not affect the cluster formation in charged microdroplets.

For the synthesis of ES Ag@BSA, $AgNO_3$ was used as the starting material. The silver cluster was prepared by keeping Ag and protein concentrations the same as those used for the gold cluster. For the silver cluster, $NaBH_4$ was used as an external reducing agent.[29] For comparison of the ES product with the SP sample, similar concentrations of the gold/silver and proteins were used. To clarify that the reaction occurred in droplets and not in bulk, a mixture of $HAuCl_4$ and BSA (protein in aq. NaOH) was kept without spraying and the product was compared with the ES sample. For comparison of luminescence, the mixture was kept without spraying for 1 h which was similar to the total time duration to complete the electrospray process and process the reaction product to get it into solution. An equal volume of the mixture was taken for electrospray as well as for bulk reaction. While the ES sample shows luminescence, the bulk mixture did not show it (Figure S2). Both the samples had equal time for interaction. Therefore, we concluded that the reaction occurred in the charged droplets, and there was no formation of Au@BSA cluster before the mixture was sprayed. In all of our experiments, we have used the single nozzle spray where the reactants were mixed and sprayed immediately after mixing. A control experiment was performed to check the effect of electrospray on the formation of clusters. In the absence of an applied field, when high-pressure nebulizing gas (N_2) was employed for the reaction, no cluster formation was noticed. The reaction leads to the formation of nanoparticles (Figure S3) that show characteristic plasmonic features for Au and Ag (Figure S4). Figure 2A shows the optical absorption feature of ES Au@BSA along with its luminescence feature. UV−Vis spectra show characteristic absorption of a PPC. Usually, in PPCs, the plasmonic feature of Au/Ag disappears, and there are no distinct absorption features. However, a slight hump appears at 280 nm, which corresponds to the features of aromatic amino acids in the protein. The UV−vis spectra of PPCs are dominated by protein features and features of the cluster core on the other hand are not clearly visible in these spectra as reported in the literature.[27] For this reason, UV−vis spectra of PPCs have not been correlated to the atomicity of the cluster, unlike that of monolayer protected clusters, where these features are more pronounced. A comparison of the UV−Vis spectra of Au_{30}@BSA synthesized by both the SP and ES methods shows similarities in them (Figure S5).

PL features of these ES clusters show emission in the range of 670−685 nm. ES Ag@BSA and ES Au@Lyz show emission maxima at 678 and 684 nm, respectively (Figure S6), whereas ES Au@BSA shows a maximum at 678 nm (Figure 2A). Multiple peak maxima are attributed to the different cluster size distributions or the presence of different chemical environments of the metal core. The excitation wavelength for all these clusters is 365 nm. The inset in Figure 2A displays the photographic image of intense red luminescent ES Au@BSA. The presence of a cluster was further strengthened by XPS analysis, which indicates the presence of a metallic core and proves the absence of metal complexes. In XPS, features at 84.2 and 87.9 eV correspond to $4f_{7/2}$ and $4f_{5/2}$ of a Au (0) core

https://doi.org/10.1021/acssuschemeng.0c09145
ACS Sustainable Chem. Eng. 2021, 9, 4554−4563

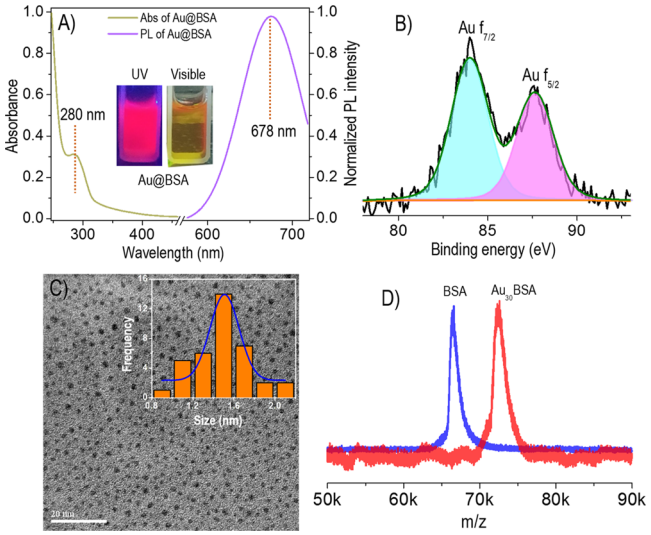

Figure 2. (A) UV−Vis spectrum (left) and PL spectrum (right) of ES Au@BSA. (B) X-ray photoelectron spectrum of ES Au@BSA in the Au 4f region, showing Au (0) oxidation state in the clusters. (C) TEM image of ES Au@BSA cluster with the inset showing the size distribution of these clusters. An average size of 1.5 nm is shown. Clusters show beam-induced damage, and the core size shown is not a true reflection of the cluster size. (D) MALDI MS of BSA and ES Au_{30}BSA. BSA shows a peak at 66,463 Da, and the cluster exhibits a feature at 72,375 Da. The difference between protein and cluster peak is equivalent to 30 Au atoms.

(Figure 2B). There is a slight shift in the binding energy toward a higher value possibly due to the reduced size of the core. Similarly, the Ag (0) core of the cluster was confirmed by peaks at 368.2 and 373.5 eV due to $3d_{5/2}$ and $3d_{3/2}$ of Ag (0), respectively (Figure S7). The spectrum for Ag (0) has a higher binding energy component, which may be assigned to the positively charged silver atoms chemically bonded to the sulfur atoms of the thiol groups present in the protein.[60]

The spectrum for Ag (0) has a higher binding energy component, which may be assigned to the smaller clusters or surface atoms of a cluster. The XPS feature around 163 eV is attributed to $2p_{3/2}$ of sulfur, which is characteristic of thiolate binding to the Au/Ag core (Figure S8). Therefore, it is clear that the core of the cluster is stabilized by the thiol groups of proteins. The TEM image has shown (Figure 2C) the presence of nanometer-sized clusters. Protein-protected Au or Ag nanoclusters with a small core size are ultrasmall nanoparticles and are typically below 2 nm in diameter. However, the size distribution of the cluster from the TEM image presents an average size of 1.5 nm. This is because these clusters are sensitive toward the high-energy electron beam, and nanoparticles were formed due to the aggregation of clusters caused by continuous irradiation of the beam. This has been studied in detail in the past.[61] TEM images of ES Ag@BSA and ES Au@Lyz are shown in Figure S9. Molecular nature of the ES Au@BSA cluster was confirmed by the MALDI mass spectrum. Figure 2D displays the mass spectrum of the protein, BSA, along with that of the gold cluster. The spectra were collected in the positive mode. The mass spectrum of BSA shows a distinct peak at m/z of 66,463 Da due to a mono-cation. We have observed another distinct feature for our ES Au@BSA cluster at m/z of 72,375 Da. The difference between the cluster peak and parent protein peak is equivalent to the mass of 30 Au atoms, and hence, we have assigned this peak to a Au_{30} core encapsulated with BSA. There are 35 cysteine and 5 methionine residues in 1 BSA. This favors the formation of a Au_{30} core inside a BSA molecule. This cluster was previously reported and studied with different techniques.[27,62,63] We followed the same ratio of metal ion/protein concentration during electrospray synthesis. As a result, the Au_{30} core was formed. No other cluster core was seen, and no parent protein was observed. Optical absorption features and TEM images of SP clusters were used as a reference to confirm the molecular nature of ES Ag@BSA and ES Au@Lyz (Figure S10).

Stability of the ES clusters was measured over a period of about 6 months. No significant change was noticed in stability when measured at an interval of 30 days. After 6 months, almost 90% of the luminescence intensity was intact in these clusters (Figure S11A). The retention of PL properties for such a long time enables its utility for bioimaging and sensing. Biocompatibility of the clusters made them useful to work effectively in the biological medium for which understanding the stability of these clusters over varying pH ranges is essential. As these clusters are encapsulated in proteins, the effect of pH on the capping is more prominent than the cluster core. Figure S11B shows the change in luminescence intensity at varying pH. When the solution was changed from acidic to alkaline medium, there was an increase in the luminescence intensity of the clusters. This is because tyrosine (Tyr) residues in the protein can reduce Au (III) ions through their phenolic groups, and their reduction capability can be greatly improved by adjusting the pH of the reaction above the pK_a of Tyr (~10).[9] We observed an increase in luminescence intensity

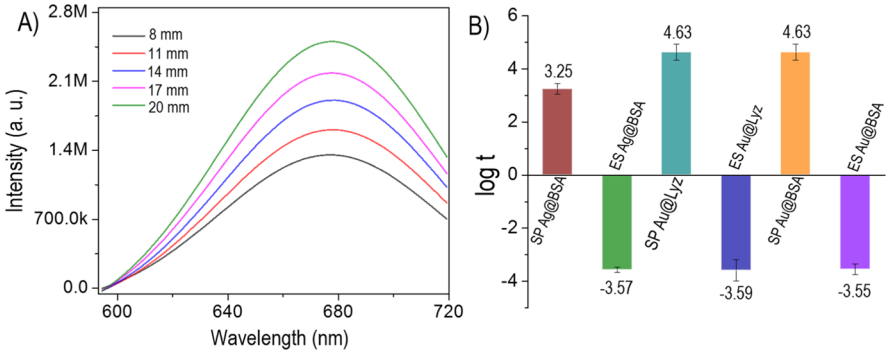

Figure 3. (A) Distance-dependent luminescence measurement to show the formation and origin of luminescence of ES Au@BSA clusters in microdroplets. (B) Comparison of the total time required for the synthesis of clusters (in terms of log scale) in the solution phase as well as by electrospray.

https://doi.org/10.1021/acssuschemeng.0c09145
ACS Sustainable Chem. Eng. 2021, 9, 4554−4563

while changing the pH from acidic to alkaline as evident from Figure S11B.

3.2. Origin of Luminescence and Enhanced Rate of the Reaction. To prove the origin of luminescence in droplets, distance-dependent luminescence measurements were performed. Solutions of the same concentrations were electrosprayed for the same time at different distances (d), and luminescence was measured. With an increase in distance, d, enhancement in luminescence was noticed (Figure 3A). The reason for such an enhancement could be the enhanced reactivity in the droplets as the reactants get more time to react when the distance goes on increasing. We have further increased the tip to substrate distance (up to 32 mm) to check its effect on luminescence (Figure S12). From the experiment, we have observed that up to a certain distance, luminescence is increasing but the increase is not linear. This may be due to the fact that during the electrospray process, solvent evaporation occurs and the droplet concentrates with an increase in distance. This may lead to self-quenching of the luminescent material in the droplets or it may be quenched due to the presence of water (solvent), which is a well-known quencher. Increasing the distance beyond a certain point shows that luminescence is almost constant. This may be due to the fact that after a certain distance, the reaction comes to an end as a result of the complete evaporation of the droplet.

We have compared the time required for the solution-phase synthesis of clusters with that of ES clusters. The reaction time for the formation of ES clusters is the same as the time of travel of the droplets from the nozzle tip to the solid substrate. The reaction time for the traveling droplets was adjusted by varying the distance between the tip to the substrate. The movements of the droplets were recorded using a high-speed camera at 400,000 frames per second (fps) (Figure S13). The time gap between two images is 2.5 μs. The velocity distribution of the microdroplets was determined by tracking 20 individual droplets. The velocity distribution of the microdroplets was fitted with a straight line which shows a constant velocity of the droplets during the reaction (Figure S14). The detail of the velocity calculation is discussed in the Supporting Information. The estimated reaction time was calculated by integrating the speed of the microdroplets over the travelling distance. The travelling time, that is, the time of product formation for ES Au@Lyz, ES Ag@BSA, and ES Au@BSA, were calculated as 260.9, 267.5, and 282.0 μs, respectively, whereas in the solution phase, the time required for the formation of these clusters was 12 h, 30 min, 12 h, respectively. These SP clusters are termed as SP Au@Lyz, SP Ag@BSA, and SP Au@BSA, respectively. Figure 3B shows the plot of the comparison of time required for the synthesis of clusters in the solution phase as well as by electrospray, plotted on a logarithmic scale. For SP clusters, the time required was several hours and hence shows a value in the positive axis. However, the ES clusters require very little time, of the order of microseconds and show a value in the negative axis, which is evident from the graph. The rate of enhancement of reactions can be calculated by taking an antilog of the difference between the values for both processes. The values of the rate of enhancement of the reaction in droplets for ES Ag@BSA, ES Au@Lyz, and ES Au@BSA, respectively, were 6.72×10^6, 1.65×10^8, and 1.53×10^8 times faster than that of SP synthesis. Synthesis of protein-protected clusters at such a fast rate is an exciting phenomenon because during this small time scale, several processes, such as reduction of Au^{3+} to Au, conformational changes in proteins, the formation of metal–protein complex, aggregation of the gold atoms to form clusters, and any other event involved in forming a stable cluster, occurs. As the process is extremely fast, it is difficult to perform spectroscopy on the droplets and understand the phenomena happening in single droplets. Hence, the complete mechanism of the reaction is uncertain.

3.3. Enhancement of Luminescence Using Droplets. For a given concentration of the reactants, when luminescence of clusters prepared by both the methods were compared, we observed an enhancement in luminescence for the ES cluster. ES Au@BSA shows 2-fold enhancement in luminescence, whereas ES Ag@BSA and ES Au@Lyz show 1.2- and 1.6-fold enhancement, respectively (Figure 4). In order to make this

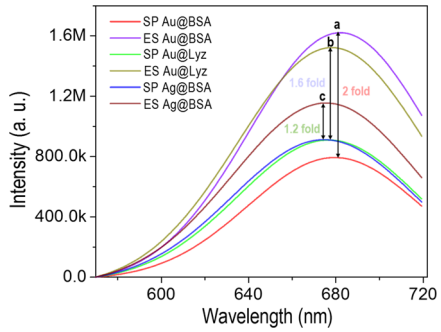

Figure 4. Comparison of luminescence of ES clusters with the SP clusters for a given concentration. ES clusters show 2-fold, 1.6-fold, and 1.2-fold enhancement in luminescence for ES Au@BSA, ES Au@Lyz, and ES Ag@BSA, respectively, compared to SP clusters.

comparison, the amount of clusters used and all other parameters such as volume, temperature, pH, excitation wavelength, age of the samples, and spectrometer parameters were held the same.

In the solution phase, the reactant gets enough time to react and form luminescent clusters, but in droplets, the interaction time between the reactants is less. Such a small interaction time leading to luminescence enhancement is intriguing. Luminescence from these clusters is strongly dependent on their physicochemical environment. There are several factors that could possibly affect luminescence; one is the unfolding of proteins in microdroplets. Some of the important factors that affect the molecular environment of the protein around the cluster core are solvents, external salts, buffers, pH, ionic strength, oxygen content, and temperature. Lee et al. have shown that cytochrome c in a slightly acidic environment can lead to conformational changes in the protein.[45] However, reports also exist on the base-induced unfolding of proteins where an increase in pH leads to the breaking of disulfide bonds.[32] During electrospray, the use of a base such as NaOH can result in the unfolding of proteins. The presence of an electric field could also break the hydrogen bonds and electrostatic interactions that result in additional unfolding. This leads to an enhancement in the metal (Au/Ag)–ligand (S) interaction responsible for charge transfer. With all these, there is an enhancement in luminescence. From the MALDI MS, we obtain a Au_{30} cluster core with the number of gold atoms higher than the previously reported Au_{25} cluster core.[9] This could also result in the enhancement of metal–ligand interaction. Another factor that possibly contributes to the enhanced luminescence is the evaporation of the solvent during the process. As the solvent evaporates, the droplets

https://doi.org/10.1021/acssuschemeng.0c09145
ACS Sustainable Chem. Eng. 2021, 9, 4554–4563

concentrate, and the reactants are in close vicinity of each other and are forced to react under the field. This results in the enhancement of luminescence in comparison to the SP method, where the reactants are in random motion and get distributed over a large volume.

Generally, noncovalent interactions make the clusters more rigid and energetically stable. Such interactions restrict the intramolecular vibrational/rotational motions, which help in increasing the radiative processes and reduce the nonradiative processes. During electrospray, protein unfolding happens that enhances the internal motions of the protein and increases the nonradiative processes leading to a reduction in luminescence of the clusters. There are two factors that enhance luminescence, whereas the other quenches luminescence. Thus, the overall enhancement is less pronounced as luminescence is a result of all these factors. Spectroscopic investigations on these fast-moving charged droplets may shed light on the possible mechanism of luminescence enhancement in these ES clusters. Figure S15 shows the comparison of QY between the ES clusters and SP clusters. It is to be noted that the measured QYs of ES Au@BSA, ES Au@Lyz, and ES Ag@BSA are 9.8, 7.2, and 4.9%, respectively, which is higher than that of SP clusters (5.2, 4.8, and 3.9%, respectively). QY values are a reflection of the enhanced luminescence in ES clusters.

3.4. Understanding the Conformational Changes of the Protein in ES Au@BSA. For understanding the secondary structure of protein during electrospray, a double derivative of FTIR was studied. We have employed the technique to understand conformational changes in the protein before and after the formation of the cluster. We have utilized only BSA, SP Au@BSA, and ES Au@BSA for the study. In FTIR studies, change in the secondary structure of the protein is reflected in the characteristic stretching and bending vibrations arising in the amide region, namely amide I (1600−1690 cm^{-1}), amide II (1480−1575 cm^{-1}), amide III (1229−1301 cm^{-1}), and amide A (3300 cm^{-1}). The band close to 1650 cm^{-1} is due to the C═O stretching vibration and out of plane C−N stretching, a signature of amide I region. Amide II region is attributed to the N−H bending vibration. A broad feature around 3000−3300 cm^{-1} corresponds to the amide A region and is attributed to the N−H or O−H stretching vibration. Figure S16 shows the FTIR spectra of BSA and ES Au@BSA. As the amide I region is more sensitive to the secondary structure of the protein, we have performed the second derivative of IR (1600−1690 cm^{-1}). The bands in the regions of 1648−1660, 1612−1642, 1662−1688, and 1648 ± 2 are assigned to α-helix, β-sheets, β-turns, and random coils, respectively. Therefore, in the second derivative IR of BSA, the peak at 1651 cm^{-1} was assigned to α-helix and bands from 1615−1639 cm^{-1} were assigned to β-sheets. A new band appearing in the 1648 cm^{-1} range of ES Au@BSA is assigned to the random coil or unordered structure (Figure 5). On the other hand, the band at 1651 cm^{-1} is becoming featureless as we move from BSA to ES Au@BSA as the protein structure became relaxed due to the perturbation in the α-helical region. This indicates a large change in the protein structure. When compared with the FTIR of BSA, there is a change in the protein structure for the SP Au@BSA also. But no noticeable change is there in the FTIR spectra of SP Au@BSA and ES Au@BSA.

3.5. Bioimaging of Retinoblastoma Cells. Rb is an intraocular tumor that is curable if diagnosed early. The mode of treatment for Rb has changed from systemic chemotherapy

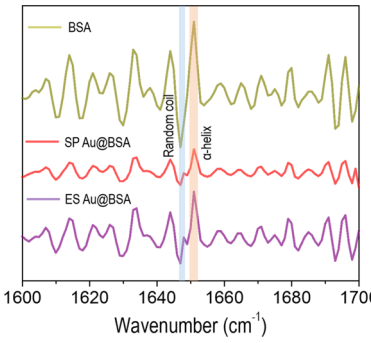

Figure 5. Second derivative FTIR spectra of BSA and ES Au@BSA. Decrease in the intensity of α-helix and the evolution of random coil nature in ES Au@BSA confirm the conformational changes in the protein after cluster formation.

to direct ophthalmic artery chemotherapy and intravitreous injection.[64,65] Success has been achieved in ocular survival, but treating the tumors that grow from the retina to the vitreous humor, namely vitreous seeds, has been more difficult to cure and may relapse. On the basis of the appearance in fundoscopy, these vitreous seeds were classified as dusts, spheres, and clouds.[66] Dusts are loose tumor cells in the vitreous, clouds are dense tumor fragments formed by translocation of the primary tumor content to the vitreous, and spheres are translucent solid tumors formed by further clonal growth of the dust or the cloud or by sprouting of the primary retinal tumor.[67] Each class of seeds required a different dose and number of intravitreal injections. Thus, imaging the Rb tumor to identify the type of seeds so that the right concentration and dose of chemotherapy can be selected is an unmet need for the treatment of Rb.

Previous studies have used topotecan, a fluorescent drug for the visualization of tumors and seeds.[68] Corson et al. have used bioluminescence imaging of luciferase-expressing human retinoblastoma cells injected into the vitreous of newborn rat eyes, but spatial and temporal development of tumors in this model has not been studied.[69] In the present study, we have used a red luminescent ES Au@BSA cluster for imaging Rb cells. Several previous studies have demonstrated the performance of SP clusters for bioimaging purposes.[70,71] Research is still evolving for improving the quantum efficiency of nanoclusters and several methods such as aggregation of nanoclusters are employed for increasing the quantum yield.[72] We made ES clusters that exhibited enhanced quantum yields compared to SP clusters. Therefore, we tested these clusters for bioimaging purposes. We have used commercial retinoblastoma cell lines NCC-RbC-51 (metastatic cell lines), which grow as loose aggregates, resembling vitreous seeds, classified as dust.[73] Before the experiment, the stability of ES Au@BSA cluster in the RPMI 1640 medium was measured. The cluster shows good stability for 40 h and no degradation was noticed (Figure S17A). Excitation at 480 nm was used for the fluorescence imaging of Rb cells (Figure S17B). Our results showed that with as low a concentration as 1 mg/ml and within 1 h of treatment, there was uptake of the nanocluster (Figure S18). This suggests that the cluster shows good penetration into the Rb cells and could be used for rapid fluorescence imaging of the cells. Rapid imaging techniques are needed in RB tumor imaging as usually patients are children below 5 years of age and longer time interval modalities are difficult to administer. This could be used as an alternative to

https://doi.org/10.1021/acssuschemeng.0c09145
ACS Sustainable Chem. Eng. 2021, 9, 4554−4563

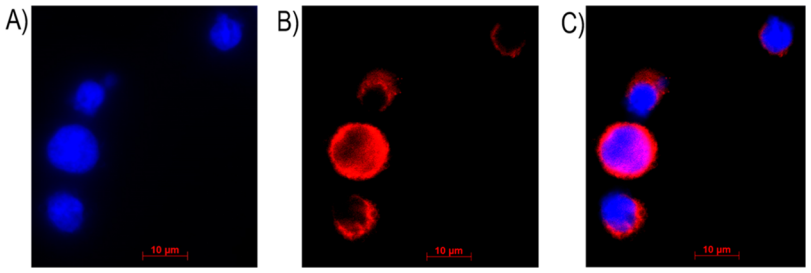

Figure 6. Fluorescence microscopic image of ES Au@BSA cluster in retinoblastoma NCC-RbC-51 cells after 24 h incubation. 1 mg/mL of cluster concentration was used for imaging. (A) Cell nucleus stained with DAPI. (B) Fluorescent image of ES Au@BSA cluster showing red luminescence inside the cells. (C) Overlay of the images, A and B showing the selective diffusion of ES Au@BSA cluster into the cytosol of the cells.

other luminescent materials which take more time for uptake and cause cell toxicity. Cellular uptake of the particles was increased up to 24 h (Figure 6). These particles are expected to be nontoxic to Rb cells as the BSA-protected noble metal clusters are known to be nontoxic to cancer cells.[41] $Ag_{18@}$BSA clusters synthesized previously by our group exhibited no toxicity to HeLa cells for a period of 24 h at varying concentrations from 2 to 10 μM.[41] The newly synthesized cluster diffused gradually into the cytosol and localized in it, in agreement with an earlier study which showed that atomically precise metal clusters localize in cytosol after 24 h.[41] The nucleus was stained with DAPI in these experiments. The results indicate that the molecular cluster can be used as an excellent probe for in vitro imaging of NCC-RbC-51 cell lines. Thus, in a clinical scenario, the synthesized clusters could be used to image the dust of vitreous seeds in Rb patients. It could also be used to identify the type of vitreous seeds present in Rb patients.

The fluorescence intensity from these clusters is generally lower than that from organic dyes. Although the luminescence intensity is less compared to that of organic dyes, these clusters show stable luminescence in cells, unlike organic dyes that undergo photobleaching. We have performed a photobleaching experiment under UV irradiation for both the cluster and a dye (rhodamine 6G) using UV irradiation (300 W, for 5 min). We have observed a slight change in the luminescence of the cluster, whereas the luminescence of the dye was significantly reduced. When the UV light was turned off, reversible photobleaching leads to a complete recovery of luminescence after 30 min for the cluster, which was not observed in the case of the dye (Figure S19). Similar reversible photobleaching for clusters was observed by Hemmateenejad et al.[74] Hence, these clusters can be used effectively for diagnosis and imaging purposes. The tumor-specific targeting of gold clusters was achieved in earlier studies by targeting specific molecules on cancer cells such as integrins and folate receptors using RGD peptides and folate-conjugated gold clusters, respectively.[75,76] Cancer cells specifically overexpress Nucleolin proteins on the cell surface. An aptamer targeting this protein, AS1411, was conjugated to the gold clusters to achieve tumor-specific targeting.[77] In future studies, we will conjugate ES clusters to EpCAM aptamer that would specifically target cancer cells.[78]

3.6. Sustainability of the Electrospray Method.

Electrospray is a simple, direct, and one-step method for the synthesis of these luminescent clusters in charged microdroplets. The synthetic method is one-pot and does not require harsh experimental conditions such as high temperature or pressure. We have employed water as a solvent and avoided the use of organic solvents. The method also uses a reduced quantity of solvents for the production of materials as compared to the solution phase. Major advantage of this method is that it minimizes the amount of reagents needed for the synthesis and hazardous reducing agents such as N_2H_4, formaldehyde, ethylene glycol, and so forth are not used. The single-step process ensures no wastage of materials during the synthesis as compared to a multistep process where processing involves loss of solvents and other chemicals. Ambient processing, use of water as the solvent, absence of hazardous reducing agents, reduced time, reduced waste of materials, and direct deposition on substrates of choice make this method a more sustainable and greener alternative to traditional methods.

The other advantage of using electrospray is that it requires only a few microseconds for the actual process of synthesis. Hence, we can synthesize larger quantities of materials in less time using the spray method as compared to the solution phase. A multinozzle spray can be used for scaling up the production of materials if required. Moreover, the synthesis of these materials can also be performed using an electrospinning machine where a larger volume of solution can be used just like the solution-phase synthesis. Hence, in terms of yield, quality of the product, and total time needed for materials production, we believe that the electrospray method is better.

4. CONCLUSIONS

In summary, we have successfully synthesized red luminescent protein-protected clusters using charged microdroplets. The molecular nature of the cluster was confirmed by MALDI MS, which revealed that ES Au@BSA has an Au_{30} core. Synthesis of the clusters in microdroplets leads to severalfold enhancement in the rate of the reaction. ES clusters show severalfold enhancement in luminescence when compared to the same clusters prepared by the conventional solution-phase method. The origin of luminescence in microdroplets was proven by measuring distance-dependent luminescence. The ES Au@BSA cluster was utilized for in vitro imaging of retinoblastoma NCC-RbC-51 cells, which will be useful for diagnosis and for detecting associated brain abnormalities.

■ ASSOCIATED CONTENT

Supporting Information

The Supporting Information is available free of charge at https://pubs.acs.org/doi/10.1021/acssuschemeng.0c09145.

Detailed description of instrumentation, spectroscopic data, and other results (PDF)

https://doi.org/10.1021/acssuschemeng.0c09145
ACS Sustainable Chem. Eng. 2021, 9, 4554−4563

AUTHOR INFORMATION

Corresponding Author

Thalappil Pradeep − *DST Unit of Nanoscience (DST UNS) and Thematic Unit of Excellence (TUE), Department of Chemistry, Indian Institute of Technology Madras, Chennai 600 036, India;* orcid.org/0000-0003-3174-534X; Phone: 91-44-22574208; Email: pradeep@iitm.ac.in; Fax: 91-44-2257 0545/0509

Authors

Sandeep Bose − *DST Unit of Nanoscience (DST UNS) and Thematic Unit of Excellence (TUE), Department of Chemistry, Indian Institute of Technology Madras, Chennai 600 036, India*

Amit Chatterjee − *Department of Nanobiotechnology, Vision Research Foundation, Sankara Nethralaya, Chennai 600006, India*

Shantha Kumar Jenifer − *DST Unit of Nanoscience (DST UNS) and Thematic Unit of Excellence (TUE), Department of Chemistry, Indian Institute of Technology Madras, Chennai 600 036, India*

Biswajit Mondal − *DST Unit of Nanoscience (DST UNS) and Thematic Unit of Excellence (TUE), Department of Chemistry, Indian Institute of Technology Madras, Chennai 600 036, India*

Pillalamarri Srikrishnarka − *DST Unit of Nanoscience (DST UNS) and Thematic Unit of Excellence (TUE), Department of Chemistry, Indian Institute of Technology Madras, Chennai 600 036, India;* orcid.org/0000-0001-5187-6879

Debasmita Ghosh − *DST Unit of Nanoscience (DST UNS) and Thematic Unit of Excellence (TUE), Department of Chemistry, Indian Institute of Technology Madras, Chennai 600 036, India*

Angshuman Ray Chowdhuri − *DST Unit of Nanoscience (DST UNS) and Thematic Unit of Excellence (TUE), Department of Chemistry, Indian Institute of Technology Madras, Chennai 600 036, India*

M. P. Kannan − *DST Unit of Nanoscience (DST UNS) and Thematic Unit of Excellence (TUE), Department of Chemistry, Indian Institute of Technology Madras, Chennai 600 036, India*

Sailaja V. Elchuri − *Department of Nanobiotechnology, Vision Research Foundation, Sankara Nethralaya, Chennai 600006, India;* orcid.org/0000-0002-9780-2717

Complete contact information is available at: https://pubs.acs.org/10.1021/acssuschemeng.0c09145

Notes

The authors declare no competing financial interest.

ACKNOWLEDGMENTS

We would like to thank the Department of Science and Technology, Government of India for constantly supporting our research program of nanomaterials. S.B., B.M., S.K.J., D.G., P.S., and A.R.C. thank IIT Madras for their research fellowships. A.C. thanks SERB/DST (Grant no- EMR/2015/000607) for a research fellowship. M.P.K. thanks MRF for a fellowship. T.P. acknowledges funding for the Centre of Excellence on Molecular Materials and Functions by IIT Madras.

REFERENCES

(1) Mathew, A.; Pradeep, T. Noble Metal Clusters: Applications in Energy, Environment, and Biology. *Part. Part. Syst. Char.* **2014**, *31*, 1017−1053.

(2) Udayabhaskararao, T.; Pradeep, T. New Protocols for the Synthesis of Stable Ag and Au Nanocluster Molecules. *J. Phys. Chem. Lett.* **2013**, *4*, 1553−1564.

(3) Jin, R.; Zeng, C.; Zhou, M.; Chen, Y. Atomically Precise Colloidal Metal Nanoclusters and Nanoparticles: Fundamentals and Opportunities. *Chem. Rev.* **2016**, *116*, 10346−10413.

(4) Jin, R. Atomically Precise Metal Nanoclusters: Stable Sizes and Optical Properties. *Nanoscale* **2015**, *7*, 1549−1565.

(5) Zheng, J.; Nicovich, P. R.; Dickson, R. M. Highly Fluorescent Noble-Metal Quantum Dots. *Annu. Rev. Phys. Chem.* **2007**, *58*, 409−431.

(6) Hassinen, J.; Pulkkinen, P.; Kalenius, E.; Pradeep, T.; Tenhu, H.; Häkkinen, H.; Ras, R. H. A. Mixed-Monolayer-Protected Au25Clusters with Bulky Calix[4]arene Functionalities. *J. Phys. Chem. Lett.* **2014**, *5*, 585−589.

(7) Chakraborty, I.; Pradeep, T. Atomically Precise Clusters of Noble Metals: Emerging Link between Atoms and Nanoparticles. *Chem. Rev.* **2017**, *117*, 8208−8271.

(8) Krishnadas, K. R.; Natarajan, G.; Baksi, A.; Ghosh, A.; Khatun, E.; Pradeep, T. Metal-Ligand Interface in the Chemical Reactions of Ligand-Protected Noble Metal Clusters. *Langmuir* **2019**, *35*, 11243−11254.

(9) Xie, J.; Zheng, Y.; Ying, J. Y. Protein-Directed Synthesis of Highly Fluorescent Gold Nanoclusters. *J. Am. Chem. Soc.* **2009**, *131*, 888−889.

(10) Xavier, P. L.; Chaudhari, K.; Baksi, A.; Pradeep, T. Protein-Protected Luminescent Noble Metal Quantum Clusters: An Emerging Trend in Atomic Cluster Nanoscience. *Nano Rev.* **2012**, *3*, 14767.

(11) Chevrier, D. M.; Thanthirige, V. D.; Luo, Z.; Driscoll, S.; Cho, P.; MacDonald, M. A.; Yao, Q.; Guda, R.; Xie, J.; Johnson, E. R.; et al. Structure and Formation of Highly Luminescent Protein-Stabilized Gold Clusters. *Chem. Sci.* **2018**, *9*, 2782−2790.

(12) Goswami, N.; Zheng, K.; Xie, J. Bio-NCs - the marriage of ultrasmall metal nanoclusters with biomolecules. *Nanoscale* **2014**, *6*, 13328−13347.

(13) Sun, C.; Yang, H.; Yuan, Y.; Tian, X.; Wang, L.; Guo, Y.; Xu, L.; Lei, J.; Gao, N.; Anderson, G. J.; et al. Controlling Assembly of Paired Gold Clusters within Apoferritin Nanoreactor for in Vivo Kidney Targeting and Biomedical Imaging. *J. Am. Chem. Soc.* **2011**, *133*, 8617−8624.

(14) Mathew, A.; Sajanlal, P. R.; Pradeep, T. Selective Visual Detection of TNT at the Sub-Zeptomole Level. *Angew. Chem., Int. Ed.* **2012**, *51*, 9596−9600.

(15) Hu, D.; Sheng, Z.; Gong, P.; Zhang, P.; Cai, L. Highly Selective Fluorescent Sensors for Hg2+ Based on Bovine Serum Albumin-Capped Gold Nanoclusters. *Analyst* **2010**, *135*, 1411−1416.

(16) Chen, T.-H.; Tseng, W.-L. (Lysozyme Type VI)-Stabilized Au8 Clusters: Synthesis Mechanism and Application for Sensing of Glutathione in a Single Drop of Blood. *Small* **2012**, *8*, 1912−1919.

(17) Wang, Y.; Chen, J.; Irudayaraj, J. Nuclear Targeting Dynamics of Gold Nanoclusters for Enhanced Therapy of HER2+ Breast Cancer. *ACS Nano* **2011**, *5*, 9718−9725.

(18) Yu, Y.; New, S. Y.; Xie, J.; Su, X.; Tan, Y. N. Protein-Based Fluorescent Metal Nanoclusters for Small Molecular Drug Screening. *Chem. Commun.* **2014**, *50*, 13805−13808.

(19) Habeeb Muhammed, M. A.; Verma, P. K.; Pal, S. K.; Retnakumari, A.; Koyakutty, M.; Nair, S.; Pradeep, T. Luminescent Quantum Clusters of Gold in Bulk by Albumin-Induced Core Etching of Nanoparticles: Metal Ion Sensing, Metal-Enhanced Luminescence, and Biolabeling. *Chem.—Eur. J.* **2010**, *16*, 10103−10112.

(20) Lin, C.-A. J.; Yang, T.-Y.; Lee, C.-H.; Huang, S. H.; Sperling, R. A.; Zanella, M.; Li, J. K.; Shen, J.-L.; Wang, H.-H.; Yeh, H.-I.; et al. Synthesis, Characterization, and Bioconjugation of Fluorescent Gold Nanoclusters toward Biological Labeling Applications. *ACS Nano* **2009**, *3*, 395−401.

(21) Zhang, A.; Tu, Y.; Qin, S.; Li, Y.; Zhou, J.; Chen, N.; Lu, Q.; Zhang, B. Gold Nanoclusters as Contrast Agents for Fluorescent and X-Ray Dual-Modality Imaging. *J. Colloid Interface Sci.* **2012**, *372*, 239−244.
(22) Zhou, W.; Cao, Y.; Sui, D.; Guan, W.; Lu, C.; Xie, J. Ultrastable BSA-Capped Gold Nanoclusters with a Polymer-like Shielding Layer against Reactive Oxygen Species in Living Cells. *Nanoscale* **2016**, *8*, 9614−9620.
(23) Wu, X.; He, X.; Wang, K.; Xie, C.; Zhou, B.; Qing, Z. Ultrasmall Near-Infrared Gold Nanoclusters for Tumor Fluorescence Imaging in Vivo. *Nanoscale* **2010**, *2*, 2244−2249.
(24) Zhang, X.-D.; Chen, J.; Luo, Z.; Wu, D.; Shen, X.; Song, S.-S.; Sun, Y.-M.; Liu, P.-X.; Zhao, J.; Huo, S.; et al. Enhanced Tumor Accumulation of Sub-2 Nm Gold Nanoclusters for Cancer Radiation Therapy. *Adv. Healthcare Mater.* **2014**, *3*, 133−141.
(25) Fernández-Iglesias, N.; Bettmer, J. Synthesis, purification and mass spectrometric characterisation of a fluorescent Au9@BSA nanocluster and its enzymatic digestion by trypsin. *Nanoscale* **2014**, *6*, 716−721.
(26) Yue, Y.; Liu, T.-Y.; Li, H.-W.; Liu, Z.; Wu, Y. Microwave-Assisted Synthesis of BSA-Protected Small Gold Nanoclusters and Their Fluorescence-Enhanced Sensing of Silver(i) Ions. *Nanoscale* **2012**, *4*, 2251−2254.
(27) Mohanty, J. S.; Baksi, A.; Lee, H.; Pradeep, T. Noble Metal Clusters Protected with Mixed Proteins Exhibit Intense Photoluminescence. *RSC Adv.* **2015**, *5*, 48039−48045.
(28) Le Guével, X.; Hötzer, B.; Jung, G.; Hollemeyer, K.; Trouillet, V.; Schneider, M. Formation of Fluorescent Metal (Au, Ag) Nanoclusters Capped in Bovine Serum Albumin Followed by Fluorescence and Spectroscopy. *J. Phys. Chem. C* **2011**, *115*, 10955−10963.
(29) Mathew, A.; Sajanlal, P. R.; Pradeep, T. A Fifteen Atom Silver Cluster Confined in Bovine Serum Albumin. *J. Mater. Chem.* **2011**, *21*, 11205−11212.
(30) Mohanty, J. S.; Xavier, P. L.; Chaudhari, K.; Bootharaju, M. S.; Goswami, N.; Pal, S. K.; Pradeep, T. Luminescent, Bimetallic AuAg Alloy Quantum Clusters in Protein Templates. *Nanoscale* **2012**, *4*, 4255−4262.
(31) Xavier, P. L.; Chaudhari, K.; Verma, P. K.; Pal, S. K.; Pradeep, T. Luminescent Quantum Clusters of Gold in Transferrin Family Protein, Lactoferrin Exhibiting FRET. *Nanoscale* **2010**, *2*, 2769−2776.
(32) Chaudhari, K.; Xavier, P. L.; Pradeep, T. Understanding the Evolution of Luminescent Gold Quantum Clusters in Protein Templates. *ACS Nano* **2011**, *5*, 8816−8827.
(33) Chan, P.-H.; Chen, Y.-C. Human Serum Albumin Stabilized Gold Nanoclusters as Selective Luminescent Probes forStaphylococcus aureusand Methicillin-ResistantStaphylococcus aureus. *Anal. Chem.* **2012**, *84*, 8952−8956.
(34) Baksi, A.; Xavier, P. L.; Chaudhari, K.; Goswami, N.; Pal, S. K.; Pradeep, T. Protein-Encapsulated Gold Cluster Aggregates: The Case of Lysozyme. *Nanoscale* **2013**, *5*, 2009−2016.
(35) Sarkar, D.; Mahitha, M. K.; Som, A.; Li, A.; Wleklinski, M.; Cooks, R. G.; Pradeep, T. Metallic Nanobrushes Made Using Ambient Droplet Sprays. *Adv. Mater.* **2016**, *28*, 2223−2228.
(36) Sarkar, D.; Mahapatra, A.; Som, A.; Kumar, R.; Nagar, A.; Baidya, A.; Pradeep, T. Patterned Nanobrush Nature Mimics with Unprecedented Water-Harvesting Efficiency. *Adv. Mater. Interfaces* **2018**, *5*, 1800667.
(37) Sarkar, D.; Singh, R.; Som, A.; Manju, C. K.; Ganayee, M. A.; Adhikari, R.; Pradeep, T. Electrohydrodynamic Assembly of Ambient Ion-Derived Nanoparticles to Nanosheets at Liquid Surfaces. *J. Phys. Chem. C* **2018**, *122*, 17777−17783.
(38) Sarkar, D.; Mondal, B.; Som, A.; Ravindran, S. J.; Jana, S. K.; Manju, C. K.; Pradeep, T. Holey MoS2 Nanosheets with Photocatalytic Metal Rich Edges by Ambient Electrospray Deposition for Solar Water Disinfection. *Glob. Chall.* **2018**, *2*, 1800052.
(39) Jana, A.; Jana, S. K.; Sarkar, D.; Ahuja, T.; Basuri, P.; Mondal, B.; Bose, S.; Ghosh, J.; Pradeep, T. Electrospray Deposition-Induced Ambient Phase Transition in Copper Sulphide Nanostructures. *J. Mater. Chem. A* **2019**, *7*, 6387.
(40) Lee, J. K.; Samanta, D.; Nam, H. G.; Zare, R. N. Spontaneous Formation of Gold Nanostructures in Aqueous Microdroplets. *Nat. Commun.* **2018**, *9*, 1562.
(41) Ghosh, D.; Bodiuzzaman, M.; Som, A.; Raja, S.; Baksi, A.; Ghosh, A.; Ghosh, J.; Ganesh, A.; Samji, P.; Mahalingam, S.; Karunagaran, D.; Pradeep, T. Internalization of a Preformed Atomically Precise Silver Cluster in Proteins by Multistep Events and Emergence of Luminescent Counterparts Retaining Bioactivity. *J. Phys. Chem. C* **2019**, *123*, 29408−29417.
(42) Müller, T.; Badu-Tawiah, A.; Cooks, R. G. Accelerated Carbon−Carbon Bond-Forming Reactions in Preparative Electrospray. *Angew. Chem., Int. Ed.* **2012**, *51*, 11832−11835.
(43) Banerjee, S.; Zare, R. N. Syntheses of Isoquinoline and Substituted Quinolines in Charged Microdroplets. *Angew. Chem., Int. Ed.* **2015**, *54*, 14795−14799.
(44) Li, A.; Luo, Q.; Park, S.-J.; Cooks, R. G. Synthesis and Catalytic Reactions of Nanoparticles Formed by Electrospray Ionization of Coinage Metals. *Angew. Chem., Int. Ed.* **2014**, *53*, 3147−3150.
(45) Lee, J. K.; Kim, S.; Nam, H. G.; Zare, R. N. Microdroplet Fusion Mass Spectrometry for Fast Reaction Kinetics. *Proc. Natl. Acad. Sci. U.S.A.* **2015**, *112*, 3898−3903.
(46) Dimaras, H.; Corson, T. W. Retinoblastoma, the Visible CNS Tumor: A Review. *J. Neurosci. Res.* **2019**, *97*, 29−44.
(47) Moll, A. C.; Koten, J. W.; Lindenmayer, D. A.; Everse, L. A.; Tan, K. E.; Hamburg, A.; Faber, J. A.; Den Otter, W. Three Histopathological Types of Retinoblastoma and Their Relation to Heredity and Age of Enucleation. *J. Med. Genet.* **1996**, *33*, 923−927.
(48) Orjuela, M.; Castaneda, V. P.; Ridaura, C.; Lecona, E.; Leal, C.; Abramson, D. H.; Orlow, I.; Gerald, W.; Cordon-Cardo, C. Presence of Human Papilloma Virus in Tumor Tissue from Children with Retinoblastoma: An Alternative Mechanism for Tumor Development. *Clin. Cancer Res.* **2000**, *6*, 4010−4016.
(49) Knudson, A. Retinoblastoma: Teacher of Cancer Biology and Medicine. *PLoS Med.* **2005**, *2*, No. e349.
(50) Bowles, E.; Corson, T. W.; Bayani, J.; Squire, J. A.; Wong, N.; Lai, P. B.-S.; Gallie, B. L. Profiling genomic copy number changes in retinoblastoma beyond loss ofRB1. *Gene Chromosome Canc.* **2007**, *46*, 118−129.
(51) AACR. MYCN Drives RB-Null Retinoblastoma Initiation. *Canc. Discov.* **2017**, *7*, OF13.
(52) Kyritsis, A. P.; Tsokos, M.; Triche, T. J.; Chader, G. J. Retinoblastoma-origin from a primitive neuroectodermal cell? *Nature* **1984**, *307*, 471−473.
(53) Jackson, C. G.; Glasscock, M. E., 3rd; McKennan, K. X.; Koopmann, C. F.; Levine, S. C.; Hays, J. W.; Smith, H. P. The Surgical Treatment of Skull-Base Tumors with Intracranial Extension. *Otolaryngol. Head Neck Surg.* **1987**, *96*, 175−185.
(54) Hu, Y.-C.; Chang, C.-H.; Chen, C.-H.; Ger, L.-P.; Liu, W.-S.; Lin, L.-C.; Leung, C.-M.; Chang, K.-C. Impact of Intracranial Extension on Survival in Stage IV Nasopharyngeal Carcinoma: Identification of a Subset of Patients with Better Prognosis. *Jpn. J. Clin. Oncol.* **2011**, *41*, 95−102.
(55) Abuzayed, B.; Khreisat, W.; Maaiah, W.; Agailat, S. Supratentorial Primitive Neuroectodermal Tumor Presenting with Intracranial Hemorrhage in Adult. *J. Neurosci. Rural Pract.* **2014**, *5*, 176−179.
(56) Hader, W. J.; Drovini-Zis, K.; Maguire, J. A. Primitive Neuroectodermal Tumors in the Central Nervous System Following Cranial Irradiation. *Cancer* **2003**, *97*, 1072−1076.
(57) Wang, Y.-P.; Wang, D.-J.; Niu, Z.-B.; Cui, W.-T. Chromosome 13q Deletion Syndrome Involving 13q31-qter: A Case Report. *Mol. Med. Rep.* **2017**, *15*, 3658−3664.
(58) Dryja, T. P.; Rapaport, J. M.; Joyce, J. M.; Petersen, R. A. Molecular Detection of Deletions Involving Band Q14 of Chromosome 13 in Retinoblastomas. *Proc. Natl. Acad. Sci. U.S.A.* **1986**, *83*, 7391−7394.

https://doi.org/10.1021/acssuschemeng.0c09145
ACS Sustainable Chem. Eng. 2021, 9, 4554−4563

(59) de Graaf, P.; Göricke, S.; Göricke, S.; Rodjan, F.; Galluzzi, P.; Maeder, P.; Castelijns, J. A.; Brisse, H. J. Guidelines for imaging retinoblastoma: imaging principles and MRI standardization. *Pediatr. Radiol.* **2012**, *42*, 2−14.
(60) Porcaro, F.; Carlini, L.; Ugolini, A.; Visaggio, D.; Visca, P.; Fratoddi, I.; Venditti, I.; Meneghini, C.; Simonelli, L.; Marini, C.; et al. Synthesis and Structural Characterization of Silver Nanoparticles Stabilized with 3-Mercapto-1-Propansulfonate and 1-Thioglucose Mixed Thiols for Antibacterial Applications. *Materials* **2016**, *9*, 1028.
(61) Ramasamy, P.; Guha, S.; Shibu, E. S.; Sreeprasad, T. S.; Bag, S.; Banerjee, A.; Pradeep, T. Size Tuning of Au Nanoparticles Formed by Electron Beam Irradiation of Au25 Quantum Clusters Anchored within and Outside of Dipeptide Nanotubes. *J. Mater. Chem.* **2009**, *19*, 8456−8462.
(62) Subramanian, V.; Jena, S.; Ghosh, D.; Jash, M.; Baksi, A.; Ray, D.; Pradeep, T. Dual Probe Sensors Using Atomically Precise Noble Metal Clusters. *ACS Omega* **2017**, *2*, 7576−7583.
(63) Ghosh, D.; Ganayee, M. A.; Som, A.; Srikrishnarka, P.; Murali, N.; Bose, S.; Chakraborty, A.; Mondal, B.; Ghosh, P.; Pradeep, T. Hierarchical Assembly of Atomically Precise Metal Clusters as a Luminescent Strain Sensor. *ACS Appl. Mater. Interfaces* **2021**, *13*, 6496.
(64) Chantada, G.; Schaiquevich, P. Management of Retinoblastoma in Children: Current Status. *Pediatr. Drugs* **2015**, *17*, 185−198.
(65) Francis, J. H.; Levin, A. M.; Zabor, E. C.; Gobin, Y. P.; Abramson, D. H. Ten-Year Experience with Ophthalmic Artery Chemosurgery: Ocular and Recurrence-Free Survival. *PLoS One* **2018**, *13*, No. e0197081.
(66) Munier, F. L.; Gaillard, M.-C.; Balmer, A.; Soliman, S.; Podilsky, G.; Moulin, A. P.; Beck-Popovic, M. Intravitreal Chemotherapy for Vitreous Disease in Retinoblastoma Revisited: From Prohibition to Conditional Indications. *Br. J. Ophthalmol.* **2012**, *96*, 1078−1083.
(67) Munier, F. L. Classification and Management of Seeds in RetinoblastomaEllsworth Lecture Ghent August 24th 2013. *Ophthalmic Genet.* **2014**, *35*, 193−207.
(68) Francis, J. H.; Marr, B. P.; Schaiquevich, P.; Kellick, M. G.; Abramson, D. H. Properties and Clinical Utility of Topotecan Fluorescence: Uses for Retinoblastoma. *Br. J. Ophthalmol.* **2015**, *99*, 1320−1322.
(69) Corson, T. W.; Samuels, B. C.; Wenzel, A. A.; Geary, A. J.; Riley, A. A.; McCarthy, B. P.; Hanenberg, H.; Bailey, B. J.; Rogers, P. I.; Pollok, K. E.; et al. Multimodality Imaging Methods for Assessing Retinoblastoma Orthotopic Xenograft Growth and Development. *PLoS One* **2014**, *9*, No. e99036.
(70) Zhang, L.; Wang, E. Metal Nanoclusters: New Fluorescent Probes for Sensors and Bioimaging. *Nano Today* **2014**, *9*, 132−157.
(71) Bai, Y.; Shu, T.; Su, L.; Zhang, X. Fluorescent Gold Nanoclusters for Biosensor and Bioimaging Application. *Crystals* **2020**, *10*, 357−368.
(72) Krishna Kumar, A. S.; Tseng, W.-L. Perspective on Recent Developments of near Infrared-Emitting Gold Nanoclusters: Applications in Sensing and Bio-Imaging. *Anal. Methods* **2020**, *12*, 1809−1826.
(73) Winter, U.; Aschero, R.; Fuentes, F.; Buontempo, F.; Zugbi, S.; Sgroi, M.; Sampor, C.; Abramson, D.; Carcaboso, A.; Schaiquevich, P. Tridimensional Retinoblastoma Cultures as Vitreous Seeds Models for Live-Cell Imaging of Chemotherapy Penetration. *Int. J. Mol. Sci.* **2019**, *20*, 1077−1090.
(74) Hemmateenejad, B.; Shahrivar-Kevishahi, A.; Shakerizadeh-Shirazi, F. Reversible Photobleaching of Gold Nanoclusters: A Mechanistic Investigation. *J. Phys. Chem. C* **2016**, *120*, 28215−28223.
(75) Link, S.; Beeby, A.; FitzGerald, S.; El-Sayed, M. A.; Schaaff, T. G.; Whetten, R. L. Visible to Infrared Luminescence from a 28-Atom Gold Cluster. *J. Phys. Chem. B* **2002**, *106*, 3410−3415.
(76) Li, H.; Li, H.; Wan, A. Luminescent Gold Nanoclusters for in Vivo Tumor Imaging. *Analyst* **2020**, *145*, 348−363.
(77) Chen, D.; Li, B.; Cai, S.; Wang, P.; Peng, S.; Sheng, Y.; He, Y.; Gu, Y.; Chen, H. Dual Targeting Luminescent Gold Nanoclusters for Tumor Imaging and Deep Tissue Therapy. *Biomaterials* **2016**, *100*, 1−16.
(78) Jayashree, B.; Srimany, A.; Jayaraman, S.; Bhutra, A.; Janakiraman, N.; Chitipothu, S.; Krishnakumar, S.; Baddireddi, L. S.; Elchuri, S.; Pradeep, T. Monitoring of Changes in Lipid Profiles during PLK1 Knockdown in Cancer Cells Using DESI MS. *Anal. Bioanal. Chem.* **2016**, *408*, 5623−5632.

https://doi.org/10.1021/acssuschemeng.0c09145
ACS Sustainable Chem. Eng. 2021, 9, 4554−4563